

*Chapter 4***Stereochemical Requirements of nAChR  $\alpha$ Val46 Side Chain Determined by Unnatural Amino Acid Incorporation: Support for the Pin-Into-Socket Interaction**

Reproduced in part from:

Hanek, A.P.; H.A. Lester, and D.A. Dougherty; *J. Am. Chem. Soc.* **2008**, *130* (40), 13216-13218

Copyright 2008 American Chemical Society

**4.1 Introduction**

Understanding the gating mechanism of neurotransmitter-gated ion channels constitutes one of the most significant mechanistic challenges in chemical neurobiology. For some time we have been applying the tools of physical organic chemistry to this important problem, emphasizing strategies that can produce linear free energy relationships.<sup>1,2</sup> In the present work we apply another classical tool of physical organic chemistry – the stereochemical probe<sup>3</sup> – to address a specific proposal concerning the mechanism of ion channel gating.

The nicotinic acetylcholine receptor (nAChR), like all members of the Cys-loop neurotransmitter-gated ion channel superfamily to which it belongs, mediates rapid synaptic transmission in the mammalian nervous system. At rest the nAChR is in a closed, non-conducting conformation. Upon binding of the neurotransmitter acetylcholine, the protein undergoes a conformational change to an open ion-conducting state, thereby converting the chemical signal to an electrical one.

The muscle-type nAChR is comprised of five homologous subunits ( $\alpha_1$ - $\gamma$ - $\alpha_1$ - $\delta$ - $\beta_1$ ) arranged pseudo-symmetrically around a central ion-conducting pore. Each individual

subunit has a large extracellular N-terminal domain, four membrane-spanning helices (M1–M4), and a short extracellular carboxy-terminal tail (Figure 4.1). The extracellular domain is comprised largely of  $\beta$  strands connected by short loops, with the agonist binding sites located at the  $\alpha/\gamma$  and  $\alpha/\delta$  subunit interfaces. The channel gate is located in the 2<sup>nd</sup> pore-lining helix (M2) some 40-60 Å from the ligand binding site. The nature of the communication between the binding site and channel gate is incompletely known.

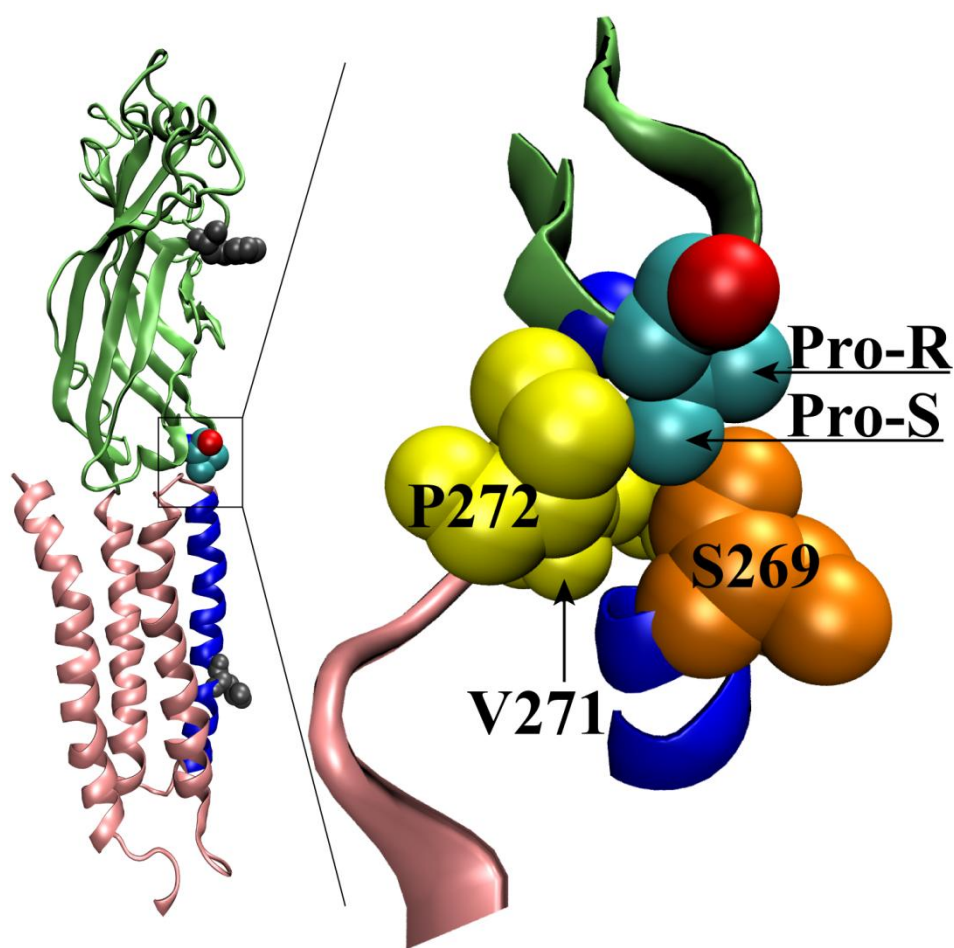


**Figure 4.1** Left: Topology of a single  $\alpha$  subunit (chain A of PDB 2BG9). The extracellular domain (green) contains the ligand binding site located at  $\alpha$ W149 (dark gray). There are four membrane-spanning helices (M1, M3, M4 in pink) including the pore-lining M2 (blue) helix containing the channel gate at  $\alpha$ L251 (dark gray). Right:  $\alpha$ Val46 (side chain in cyan, backbone carbonyl in red) is oriented such that pro-S points into a pocket formed by residues 269 (orange), 270, 271 and 272 (yellow), while the pro-R methyl points away from the pocket.

Recent cryo-EM images<sup>4,9</sup> of nAChRs from the *Torpedo* ray show that loop 2, a short loop connecting  $\beta$  strands 1 and 2, lies directly over the extracellular terminus of M2 and to one side of the M2-M3 linker (Figure 4.1). Furthermore, the structure shows that the side chain of a specific loop 2 residue in the  $\alpha$  subunit – valine 46 – points toward the top of the M2 helix.<sup>5</sup>  $\alpha$ Val46 is part of the “gating interface” between the extracellular and transmembrane domains, and we and others have argued that this interface plays an important role in communicating neurotransmitter binding to the gating region.<sup>10-18</sup> Specifically, Unwin et al.<sup>4,9</sup> propose that  $\alpha$ Val46 makes a key “pin-into-socket”<sup>7</sup> interaction, with the side chain of  $\alpha$ Val46 tucked into a hydrophobic pocket formed by the top of M2. This interaction allows  $\alpha$ Val46 to communicate changes in the structure of the extracellular domain to the M2 helix, which causes the channel gate to release. While it was immediately recognized that  $\alpha$ Val46 of the nAChR is not conserved among Cys-loop receptors,<sup>16,19</sup> and therefore that this proposed mechanism of gating cannot be conserved across the superfamily, it has also been shown that the gating mechanisms of these receptors are quite varied.<sup>11,14,16,19</sup> Therefore the proposed pin-into-socket mechanism for the nAChR merits further scrutiny.

## 4.2 Results

### 4.2.1 Unnatural Amino Acid Incorporation

To probe the hypothesis that  $\alpha$ Val46 makes a key pin-into-socket interaction, we used nonsense suppression methodology to incorporate unnatural amino acids in place of  $\alpha$ Val46. In contrast to conventional mutagenesis, unnatural amino acids allow us to perturb side chain hydrophobicity while retaining the overall size and shape of the side chain. Therefore, we can unambiguously attribute changes in receptor function to the

alterations in the polarity of the side chain with minimal concern that these subtle mutations have altered the nature of communication between the binding site and channel gate.

**Table 4.1** Measured  $EC_{50}$  values ( $\mu\text{M}$ ) for  $\alpha\text{Val46}$  mutants

Amino Acid	$EC_{50}$	$n_H$	N	Amino Acid	$EC_{50}$	$n_H$	N
Val (WT)	$50 \pm 5$	1.4	4				
Thr	>1000	---	8	<i>a</i> Thr	$102 \pm 5$	1.4	19
Ile	$58 \pm 7$	1.4	4	<i>a</i> Ile	$48 \pm 2$	1.7	8
Omt	$152 \pm 5$	1.4	12	<i>a</i> Omt	$30 \pm 1$	1.7	12

Abbreviations used: Hill coefficient ( $n_H$ ) and number of oocytes (N)

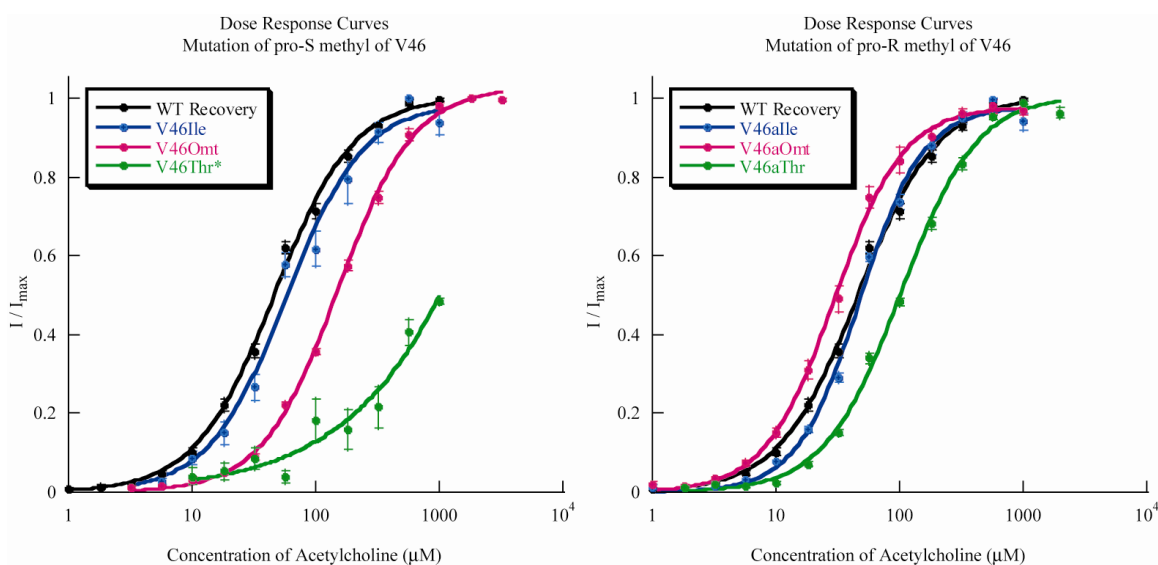


**Figure 4.2** Dose response curves for mutations at  $\alpha\text{Val46}$ . Mutations to the pro-S methyl (left panel) impact  $EC_{50}$  to a greater extent than mutations to the pro-R methyl (right panel). (\*) The Thr mutation was deleterious and the  $EC_{50}$  could not be directly measured (further discussion below).

The  $\alpha\text{Val46Thr}$  mutant was made and channel function was evaluated using whole-cell voltage clamp techniques.<sup>19</sup> Incorporation of Thr proved highly deleterious, causing a >20-fold rightward shift in  $EC_{50}$  to >1000  $\mu\text{M}$  (Table 4.1, Figure 4.2).<sup>18</sup> Threonine is isosteric to valine, thus the shift in  $EC_{50}$  must be attributed to the increase in side chain polarity. Surprisingly, incorporation of the unnatural amino acid *allo*-threonine (*a*Thr) at the same position caused only a 2-fold increase in  $EC_{50}$  (Table 4.1, Figure 4.2). Thr and

$\alpha$ Thr have the same overall side chain polarity and both are isosteric to valine, yet Thr causes a large change in channel function while  $\alpha$ Thr does not. Since the amino acids differ only in the side chain stereochemistry, the data clearly indicate that changing the polarity of the pro-S methyl of the  $\alpha$ Val46 side chain affects channel gating to a much greater extent than changing the pro-R methyl. These results and the cryo-EM image of this region suggest that the pro-R and pro-S methyl groups are in distinct environments (Figure 4.1), consistent with the pin-into-socket proposal.

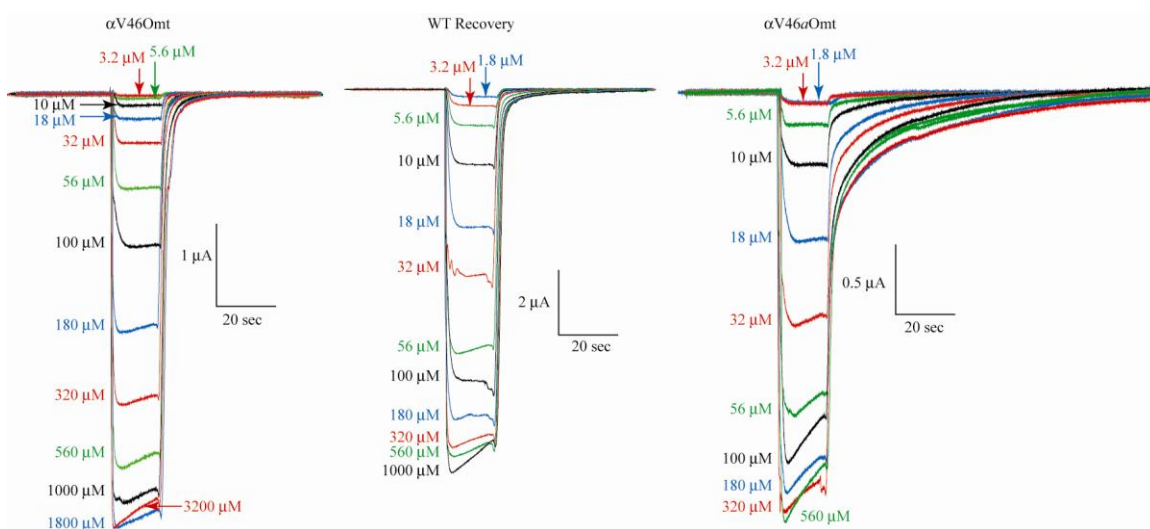


**Figure 4.3** Representative traces for wild type recovery and the Omt and  $\alpha$ Omt mutations are shown. All mutations have a sharp rise time and some desensitization once the concentration of acetylcholine exceeds the  $EC_{50}$ . The concentrations of acetylcholine are provided.

While minimally perturbing in a steric sense, converting a methyl to a hydroxyl is still a strong chemical disruption. Thus, we considered other mutants at  $\alpha$ Val46 (Table 4.1). Previously, we have employed the O-methyl threonine (Omt)/*allo*-O-methyl threonine ( $\alpha$ Omt) epimeric pair.<sup>3</sup> However, since Omt is isosteric to isoleucine, not to valine, we first incorporated isoleucine (Ile) and *allo*-isoleucine (*alle*) mutations as reference points. As expected, replacement of Val with the similarly hydrophobic Ile and

*a*Ile does not appreciably impact channel function (Table 4.1). Mutation to Omt produced a 3-fold increase in EC<sub>50</sub> to 152 μM, indicating a decrease in channel function, while *a*Omt decreased EC<sub>50</sub> slightly. Introduction of the slightly larger side chain with intermediate polarity had no effect on the macroscopic currents (Figure 4.3). These results provide an intermediate point between wild type and threonine that clearly demonstrates the importance of a hydrophobic group at the pro-S methyl of the valine side chain.

#### 4.2.2 Coupling of *α*Val46 to *β*L251

The EC<sub>50</sub> of *α*Val46Thr could not be directly measured since saturation of the whole-cell dose response curve was not achieved with 1000 μM acetylcholine. Concentrations of acetylcholine greater than 1000 μM block the whole-cell current, thus EC<sub>50</sub> values greater than 500 μM cannot be accurately measured. Previously we have used a known gain-of-function mutation, *β*L251S (Table 4.2, Figure 4.4A),<sup>3</sup> measured the EC<sub>50</sub> of the double mutant and then calculated the EC<sub>50</sub> of loss-of-function mutant.<sup>20-22</sup> The EC<sub>50</sub> of *α*Val46Thr/*β*L251S, was determined to be 74 μM (Table 4.2, Figure 4.4B). If the two mutants are independent, the EC<sub>50</sub>s are multiplicative, and the EC<sub>50</sub> of *α*Val46Thr is ~3000 μM.

**Table 4.2** Measured EC<sub>50</sub> (μM) for select *α*Val46/*β*L251S double mutations. The fold shift for the *α*Val46 single mutation is given.

<b>Mutation</b>	<b>EC<sub>50</sub></b>	<b>Fold-shift</b>	<b>n<sub>H</sub></b>	<b>N</b>
<i>β</i> L251S	1.2 ± 0.1	40.3	1.5	5
<i>α</i> Val46Thr/ <i>β</i> L251S	74 ± 5	N/A	1.6	9
<i>α</i> Val46Omt/ <i>β</i> L251S	17.5 ± 0.6	37.5	1.3	4
<i>α</i> Val46 <i>a</i> Omt/ <i>β</i> L251S	0.80 ± 0.03	8.7	1.5	4

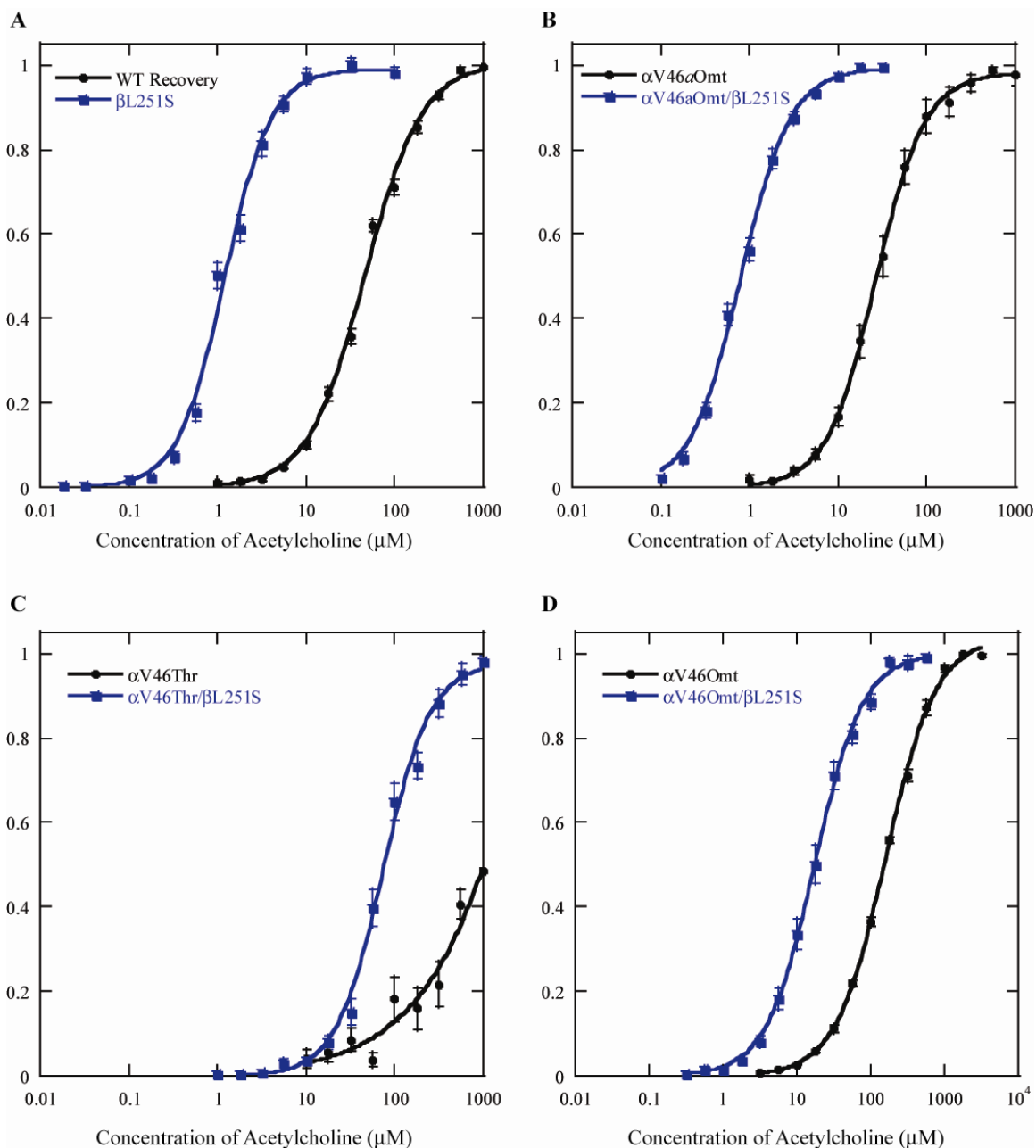


**Figure 4.4** Dose response relationship for three  $\alpha$ Val46 mutants with and without the  $\beta$ L251S mutation. **A**, The  $\beta$ L251S mutation shifts the wild type  $\text{EC}_{50}$  ~40-fold. **B**,  $\beta$ L251S shows a ~40-fold shift with the  $\alpha$ Val46 $\alpha$ Omt compared to the single mutation in the  $\alpha$  subunit. **C**,  $\alpha$ Val46Thr cannot be measured unless a second mutation ( $\beta$ L251S) is incorporated. **D**,  $\beta$ L251S does not shift the  $\text{EC}_{50}$  of  $\alpha$ Val46Omt ~40-fold.

Before assigning the  $\alpha$ Val46Thr mutant an  $\text{EC}_{50}$  of 3000  $\mu\text{M}$ , we must consider the nature of the  $\beta$ L251S mutation. This mutation is known to affect channel gating<sup>3</sup> and it has been proposed that  $\alpha$ Val46 is part of the gating pathway,<sup>4-9</sup> thus it is reasonable that

the two mutations are energetically coupled. To determine if mutations to  $\alpha$ Val46 are coupled to  $\beta$ L251S, we determined the  $EC_{50}$  of the Omt and  $a$ Omt with the  $\beta$ L251S mutation (Table 4.2). The  $a$ Omt mutation shows the characteristic  $\sim 40$ -fold shift in  $EC_{50}$  between wild type and  $\beta$ L251S (Figure 4.4B). However, the Omt mutation shows a reduced shift in  $EC_{50}$  of 8.7-fold. These results indicate that mutations to the pro-S methyl of  $\alpha$ Val46 are not independent of the  $\beta$ L251S mutation. Furthermore, these data suggest that the  $\alpha$ Val46Thr mutant is unlikely to be independent of  $\beta$ L251S, thus we cannot determine the exact  $EC_{50}$  of the Thr mutant.

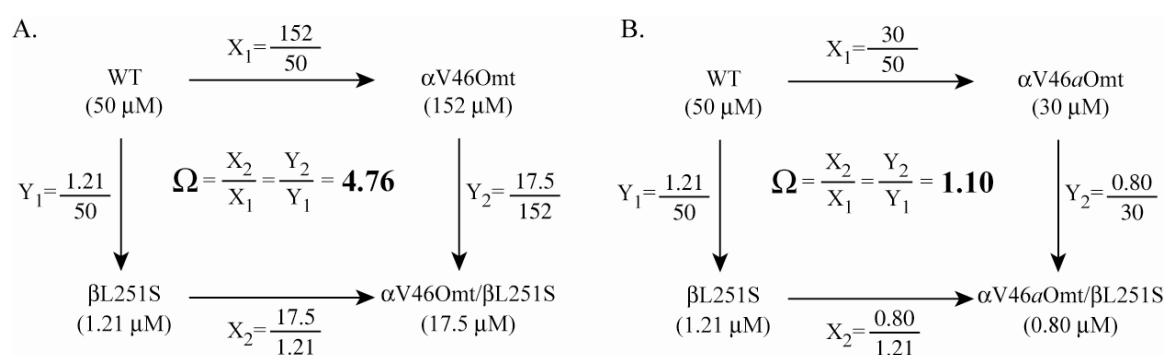


**Figure 4.5** Double mutant cycle analysis. (A)  $\alpha$ Val46Omt and  $\beta$ L251S show a coupling (i.e.,  $\Omega \neq 1$ ) while (B)  $\alpha$ Val46 $a$ Omt and  $\beta$ L251S do not.

The coupling constants,  $\Omega$ , for the Omt and  $a$ Omt mutants and  $\beta$ L251S were calculated from the double mutant cycle analysis (Figure 4.5).  $\Omega$  for two independent mutations is unity. Larger deviations from unity indicate stronger interactions, or couplings, between the two residues. The energetic coupling ( $\Delta\Delta G_{\text{int}}$ ) was calculated (Equation 4.1) and found to be 3.87 kJ/mol and 0.24 kJ/mol for Omt and  $a$ Omt, respectively.

$$\Delta\Delta G_{\text{int}} = -RT\ln(\Omega) \quad \text{Equation 4.1}$$

### 4.3 Discussion

#### 4.3.1 The Pro-S Methyl of $\alpha$ Val46 is Involved in Channel Gating

Based on the location and the subtlety of the changes, it seems unlikely that these mutations could significantly impact ligand binding events, whereas  $\alpha$ Val46 is located at the interface of the extracellular and transmembrane domains at an ideal location to influence channel gating.<sup>10-13,16,18,23</sup> Additionally, detailed kinetic studies of conventional mutations at  $\alpha$ Val46 have demonstrated that changes to this residue primarily affect gating events,<sup>11</sup> and our own data show a coupling between a known gating residue and mutations at  $\alpha$ Val46. Therefore we ascribe the changes in  $EC_{50}$  here to reflect changes in

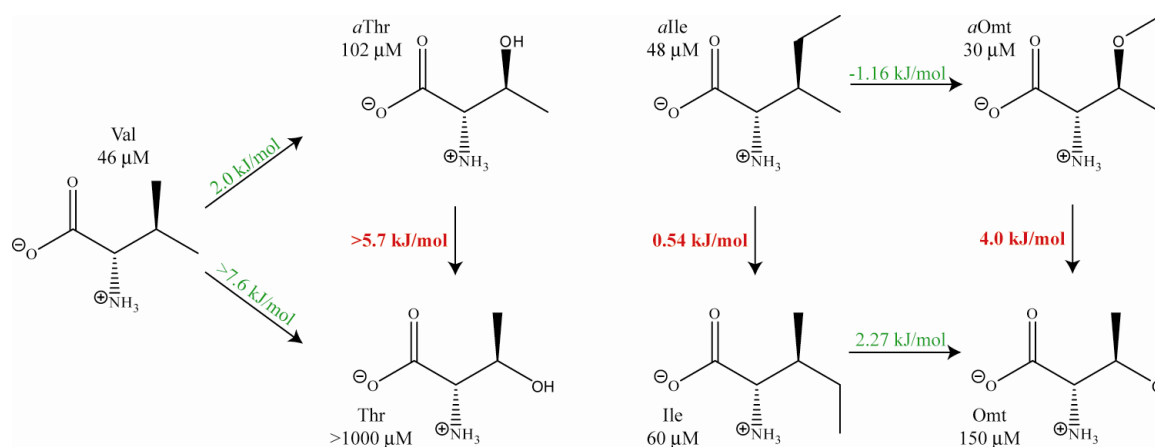


**Figure 4.6** Incorporation of polar groups in the  $\alpha$ Val46 side chain inhibits channel function to a greater extent at the pro-S position (lower row). The decreases in channel function are attributed to destabilization of the open state, stabilization of the closed state, or a combination of both.  $\Delta\Delta G$  values in red show the difference in energy for the same functional group at the pro-S versus pro-R position.  $\Delta\Delta G$  values in green show the difference in energy due to mutation from a hydrophobic to more polar group.

the gating equilibrium constant ( $k_{\text{open}}/k_{\text{closed}}$ ) for the channel. Interpreted this way (Figure 4.6), the threonine mutation at  $\alpha$ Val46 results in a greater than 7.6 kJ/mol change in the gating equilibrium. Introduction of this polar substituent affects channel gating by stabilizing the closed state, destabilizing the open state, or a combination of both.

Our results clearly indicate that the pro-S methyl group of  $\alpha$ Val46 is critical to proper channel gating, while mutation of the pro-R methyl group has little impact on channel function. Additionally, mutation to Omt shows coupling to another mutation known to affect channel gating,  $\beta$ L251S.  $\beta$ L251 is located on an entirely distinct subunit and is well-removed from the interface of the extracellular and transmembrane domains. Therefore, these two residues cannot interact directly and the energetic coupling must be the result of a long range interaction, suggesting  $\alpha$ Val46 is part of the gating pathway. Furthermore, the same interaction is not found for the  $\alpha$ Omt mutant, clearly indicating the importance of the pro-S over the pro-R methyl group. We consider the present results to provide strong support for the pin-into-socket mechanism. The images of Figure 4.1 are based on cryo-EM data that are at best of 4 Å resolution. Yet, the clear prediction that the pro-R and pro-S methyl groups of  $\alpha$ Val46 are in stereochemically distinct environments, with the pro-S tucked into a pocket, is substantially confirmed by our data.

#### *4.3.2 Consideration of Previous Studies*

Previous studies of Val46 by conventional mutagenesis<sup>11,16,23</sup> largely support the pin-into-socket interaction. Xiu et al.<sup>18</sup> found that mutation to Ala is highly deleterious, as measured by  $EC_{50}$ . A detailed kinetic analysis of the same mutation by Chakrapani et al.<sup>11</sup> revealed that the Ala mutation decreased  $k_{open}$  drastically, consistent with the proposed pin-into-socket mechanism.<sup>4-9</sup> Additionally, Xiu et al.<sup>18</sup> report data on mutations to Asp, Glu, Arg, and Lys. Mutations to Asp and Glu result in surface expressed but nonfunctional channels, while mutations to Arg and Lys increase the  $EC_{50}$  2-fold and decrease the  $EC_{50}$  30-fold, respectively. In the context of the pin-into-socket mechanism, the deleterious nature of the Asp and Glu mutations are not surprising. The

more complex issue is that of the Arg and Lys mutations. Both these residues have much longer side chains than Val and these side chains may adopt a variety of conformations such that it is possible that part of the side chain makes the same contacts necessary for channel function while keeping the positively charged portion of the side chain away from this same area of the protein. Mutations to Asp, Glu, Arg, and Lys eliminate the  $\beta$ -branching nature of WT Val, and change the size and polarity of the residues, making it difficult to attribute the changes in  $EC_{50}$  to only one of these alterations.

In addition to considering previous studies of conventional mutations, we must consider the nature of the interacting partner(s) for the pro-S methyl of Val46. Based on mutant cycle analysis using much more structurally perturbing conventional mutants, Lee and Sine suggest that a hydrophobic interaction between  $\alpha$ Val46,  $\alpha$ Ser269 and  $\alpha$ Pro272 exists.<sup>16</sup> Single-channel analyses by Jha et al. suggest that Ser269 and Ala270 move early in the gating process – contemporaneously with Val46 – while Pro272 moves later.<sup>23</sup> This could be interpreted to indicate that Val46 is more likely to interact with Ser269/Ala270. We have made no effort here to identify the interacting partner of Val46. We do note, however, that assuming the image of Figure 4.1 is of the closed state, the assignment of the pocket as being hydrophobic<sup>5,8</sup> seems inconsistent with our data. Changing the pro-S methyl to a polar group apparently stabilizes the closed state relative to the open state (raising  $EC_{50}$ ); therefore a polar pocket to receive that polar group is more consistent with our data. This pocket could be formed by backbone carbonyls and/or the side chain of S269.

As noted above, Val46 is not conserved in the Cys-loop superfamily, and so the key interaction probed here cannot play a critical gating role in all Cys-loop receptors.<sup>14,18</sup>

As discussed in detail elsewhere, this is more nearly the norm, rather than the exception, with most pairwise interactions in the crucial gating interface not being conserved across the family.<sup>12-18,23</sup> For example, Lummis et al. found that the *cis-trans* isomerization of a semi-conserved proline residue in the 5HT<sub>3A</sub>R plays a key role in the gating of this channel.<sup>17</sup> However, in the nAChR, mutation of this same proline to serine, alanine, and glycine results in functional channels, demonstrating that *cis-trans* isomerization of this proline cannot wholly account for the gating of nAChR.<sup>2,17</sup> One candidate for a conserved gating interaction is a proposed salt bridge between the residue adjacent to Val46 on loop 2 ( $\alpha$ Glu45) and a conserved Arg residue in the preM1 region. Several studies have evaluated its possible role in nAChR function, but it has not been evaluated in other Cys-loop receptors.<sup>16,18,23</sup>

#### 4.3.3 Conclusions

We conclude that, in the nAChR,  $\alpha$ Val46 does play a key role in receptor gating by a pin-into-socket mechanism, whereby the pro-S methyl group is nestled into a pocket at the top of the M2 helix. In addition to validating an intriguing feature of the cryo-EM images of this receptor, the present results further illustrate the power of unnatural amino acid mutagenesis to study the complex proteins of neuroscience using the techniques of physical organic chemistry.

## 4.4 Materials and Methods

### 4.4.1 Preparation of mRNA and Unnatural Amino Acyl-tRNA

*Conventional Mutations and mRNA synthesis:* Mutations were incorporated by Quickchange mutagenesis protocol (Stratagene) into the cDNA of the appropriate subunit gene in the pAMV vector. The mRNA coding for the mouse muscle type nAChR

subunits ( $\alpha$ ,  $\beta$ ,  $\gamma$ , and  $\delta$ ) was obtained by linearization of the expression vector (pAMV) with NotI (Roche), followed by *in vitro* transcription using mMessage mMachin kits (Ambion, Austin, TX).

*Preparation of Amino acyl tRNA:* 74 nt tRNA was made by runoff transcription using a T7 Megashortscript kit from Ambion (Austin, TX). 30  $\mu$ g of 74 nt tRNA is dissolved to 45  $\mu$ l in 10 mM HEPES. The tRNA/HEPES mixture is placed in boiling water to denature and then cooled to 37°C in a water bath. 12  $\mu$ L of 3 mM (in DMSO) dCA-Uaa, 48  $\mu$ L of 2.5X reaction mix, 7.8  $\mu$ L water, and 7.2  $\mu$ L of T4 RNA ligase (New England BioLabs) is added to the tRNA/HEPES mixture. The reaction is incubated for 45 minutes in a 37°C water bath. The reaction is quenched by addition of 12.5  $\mu$ l of NaOAc (3.0 M, pH=5.0) and 17.5  $\mu$ l of water. The ligated tRNA-Uaa is purified by 25:24:1 Phenol:chloroform:isoamyl alcohol (PCI) extraction (150  $\mu$ l) followed by a back extraction of the PCI layer using 6.3  $\mu$ l NaOAc (3.0 M, pH=5.0) and 68.7  $\mu$ l water. The aqueous layers are combined and extracted with 24:1 chloroform:isoamyl alcohol (225  $\mu$ l). 675  $\mu$ l of ethanol is added to the aqueous layer and the mixture is left to precipitate overnight at -20°C. The tRNA-Uaa is pelleted by spinning at 1400 RPM for 20 minutes at 4°C. The supernatant is removed and the pellet dried in a dessicator for 20 minutes. The pellet is redissolved in 25  $\mu$ l of 1 mM NaOAc, pH=4.5, checked by MALDI and quantified by UV/Vis.

#### 4.4.2 Electrophysiology and Data Analysis

*Two electrode voltage clamp:* For conventional mutants, mRNAs of  $\alpha$ ,  $\beta$ ,  $\gamma$  and  $\delta$  subunits were mixed in the ratio of 2:1:1:1 and microinjected into stage VI oocytes of

*Xenopus laevis*. Electrophysiology recordings were performed 24-48 hours after injection in two-electrode voltage clamp mode using the OpusXpress 6000A. The clamping voltage was -60 mV and agonist was applied for 15 seconds. Acetylcholine chloride was purchased from Sigma/Aldrich/RBI (St. Louis, MO). All drugs were diluted to the desired concentrations with calcium-free ND96 buffer. Dose-response data were obtained for at least 8 concentrations of agonists and for a minimum of 5 oocytes. Mutants with  $I_{\max}$  equal to or greater than 400 nA are regarded to be functional.  $EC_{50}$  and Hill coefficient were calculated by fitting the dose response relation to the Hill equation (Equation 4.2), where  $I_{\max}$  is the maximal current,  $EC_{50}$  is the effective concentration to elicit a half maximal response, and  $n$  is the Hill coefficient. All data are reported as means  $\pm$  S.E.

$$I = \frac{I_{\max}}{1 + EC_{50}/[A]^n} \quad \text{Equation 4.2}$$

If saturation was not reached at 1000  $\mu$ M concentrations of acetylcholine, the  $EC_{50}$  could not be calculated. For the  $\alpha$ V46Thr mutant, a second mutation known to consistently reduce the wild type  $EC_{50}$  to 1.2  $\mu$ M<sup>3</sup> was introduced. The second mutation incorporated a leucine to serine mutation in the  $\beta$  subunit ( $\beta$ L251S). The  $EC_{50}$  of the double mutant was then determined as described. The  $EC_{50}$  of the single mutant is calculated by multiplying the  $EC_{50}$  of the double mutant by 42 (50/1.2).

*Unnatural amino acid suppression:* The aminoacyl tRNA was deprotected by photolysis immediately prior to co-injection with mRNA containing an *amber* (TAG) stop codon at the site of interest. The mRNA is mixed in a 10:1:1:1 mixture and co-injected with an equal volume of tRNA-Uaa. Recovery of WT and the conventional

mutation V46I were employed as positive controls. Co-injection of mRNA with 76 nt tRNA (no Uaa) was used to test for re-aminoacylation at this site. This negative control showed no response to 1 mM ACh. An additional negative control of mRNA only (read-through) also showed no response to 1 mM ACh.

*Energy Calculations:*  $\Delta\Delta G$  values for Figure 4.6 were calculated using Equation 4.3. These calculations assume that the mutations affect the gating equilibrium but not the binding equilibrium, as evidenced by other studies at this site.<sup>11</sup>

$$\Delta\Delta G = RT \ln \left( \frac{EC_{50}(\text{mutant})}{EC_{50}(\text{wt})} \right) \quad \text{Equation 4.3}$$

#### 4.4.3 Unnatural Amino Acid Preparation

The amino acids isoleucine, allo-isoleucine, O-methyl threonine, and allo-O-methyl threonine were previously prepared,<sup>3,24</sup> with NVOC protection and cyanomethyl ester activation followed by coupling to dCA as described.<sup>19</sup>

*NVOC allo-threonine:* 381 mg (3.6 mmol) of Na<sub>2</sub>CO<sub>3</sub> and 3.8 mL of water was stirred to make a 10% weight/volume mixture. 115 mg (0.96 mmol) of allo-threonine (Aldrich) was added to this mixture. The entire reaction was then put on ice. NVOC-Cl (278 mg, 1.01 mmol) was added while stirring. The ice was removed and the reaction allowed to warm to room temperature. The reaction was monitored by TLC. After 5 hours the reaction was complete. 50 mL of water was added, turning the reaction cloudy and yellow. 3 x 20 mL of ether was used to wash the aqueous layer. The aqueous layer (clear, yellow) was acidified with 6N HCl to pH < 2. The product was extracted into ether (3 x 25 mL), and the organic layer was dried over MgSO<sub>4</sub>. MgSO<sub>4</sub> was removed by filtration and the organic solution was concentrated under reduced pressure to give a

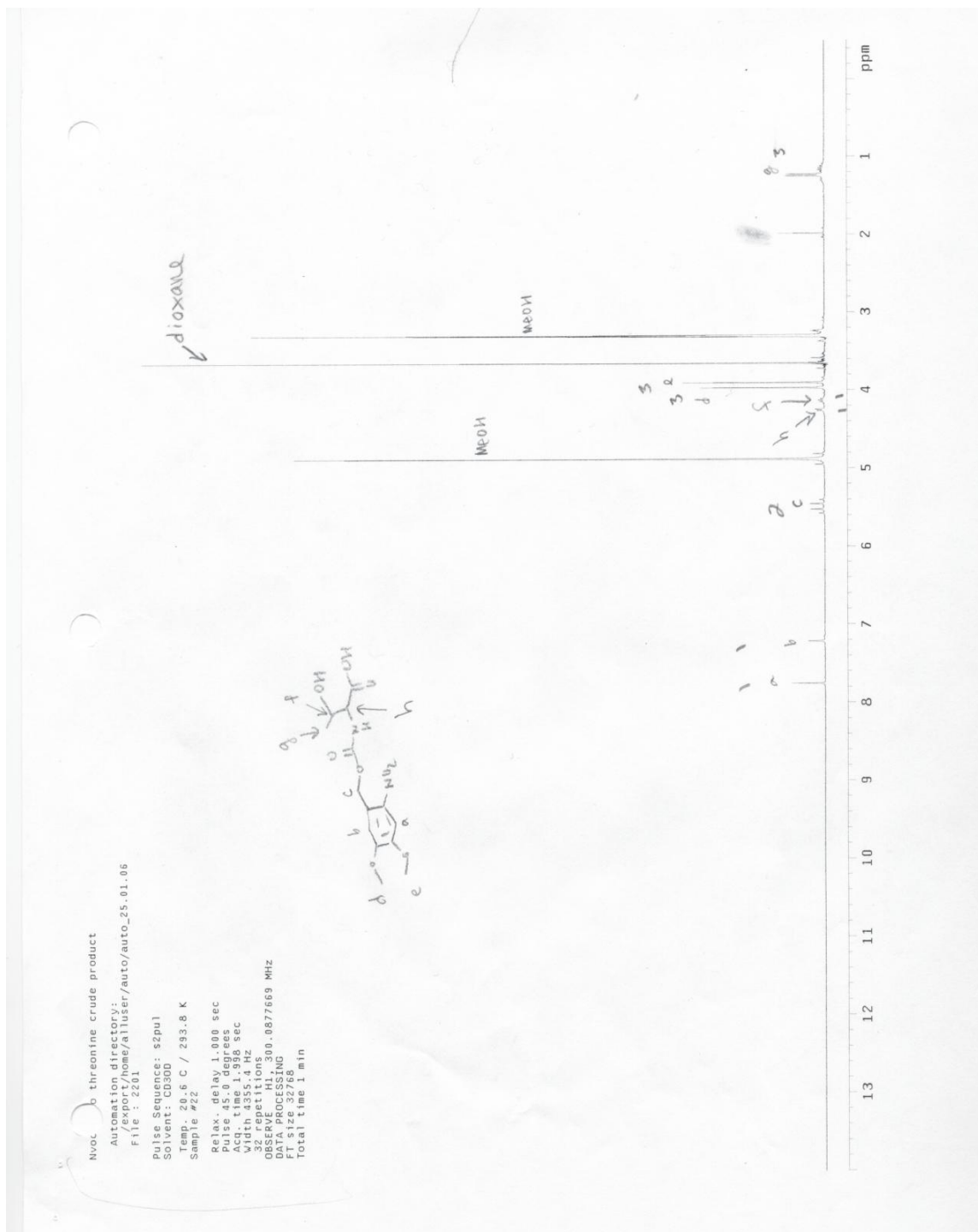
yellow oil (330 mg). MS gives a peak at 380.8 consistent with the mass of NVOC-*a*Thr plus a sodium ion. Proton NMR (300 MHz, Figure 4.7) in CD<sub>3</sub>OD gives peaks at 7.75 (s, 1H), 7.21 (s, 1H), 5.48 (q, 2H), 3.97 (s, 3H), 3.91 (s, 3H), 4.14 (t, 1H), 1.23 (d, 3H), and 4.25 (d, 1H). Yield 229 mg (0.64 mmol), 66.5%

*Cyanomethyl ester of NVOC-aThr*: 229 mg (0.64 mmol) of NVOC-*a*Thr was added to a dry flask that was then purged with argon. 2 mL of dry DMF followed by 2 mL (32 mmol) of chloroacetonitrile, and 0.25 mL (1.92 mmol) of triethylamine were added. The reaction was clear and yellow prior to addition of triethylamine. The reaction was stirred under argon and monitored by TLC. After 3 hours, the solvent was removed (vacuum line, overnight) leaving a yellow/brown solid. The solid was dissolved in methylene chloride and purified on a silica gel column using a gradient of ethyl acetate and methylene chloride. All fractions were spotted on a TLC plate and combined according to their contents. The solvent was removed. The desired product forms a white, needlelike solid that is highly insoluble. Positive ion MS gives peaks at 419.6 and 435.6 consistent with a mass of 396.6 for the product plus the mass of Na and K, respectively. Proton NMR (300 MHz, Figure 4.8) in CDCl<sub>3</sub> gives peaks at 7.72 (s, 1H), 6.99 (s, 1H), 5.55 (d of d, 2H), 4.01 (s, 3H), 3.96 (s, 3H), 4.21 (m, 1H), 1.33 (d, 3H), 4.48 (d of d, 1H), 4.82 (d of d, 2H), and 5.76 (d, 1H). Yield 117 mg (0.295 mmol), 46%.

*Allo-threonine coupling to dCA*: 10 mg (0.025 mmol) of the cyanomethyl ester NVOC-*a*Threonine was dissolved in 0.6 mL of DMF under argon. Once dissolved, 10 mg (0.008 mmol) of dCA and 4.85 mg (0.020 mmol) of tetrabutylammonium chloride were added, and the reaction was stirred under argon, overnight. The reaction was quenched with 1:1 water:acetonitrile, filtered and purified by HPLC. Fractions

containing the dCA- $\alpha$ Thr-NVOC (as determined by the ratio of peaks at  $\lambda=350$  nm and  $\lambda=260$  nm) were combined. The solvent was removed by lyophilization. The remaining solid was dissolved in 15 mL of 10 mM acetic acid, flash frozen and the solvent was removed by lyophilization. This step was repeated 3 times. The dCA- $\alpha$ Thr-NVOC was confirmed by MALDI-TOF ( $m/z = 975.6$ ).

## 4.5 Proton NMR Spectra

Figure 4.7 Proton NMR of NVOC-*a*Thr



## 4.6 References

- (1) Dougherty, D. A. *Chem Rev* **2008**, *108*, 1642-53.
- (2) Dougherty, D. A. *J Org Chem* **2008**, *73*, 3667-73.
- (3) Kearney, P. C.; Zhang, H.; Zhong, W.; Dougherty, D. A.; Lester, H. A. *Neuron* **1996**, *17*, 1221-9.
- (4) Miyazawa, A.; Fujiyoshi, Y.; Stowell, M.; Unwin, N. *J Mol Biol* **1999**, *288*, 765-86.
- (5) Miyazawa, A.; Fujiyoshi, Y.; Unwin, N. *Nature* **2003**, *423*, 949-55.
- (6) Unwin, N. *Novartis Found Symp* **2002**, *245*, 5-15; discussion 15-21, 165-8.
- (7) Unwin, N. *FEBS Lett* **2003**, *555*, 91-5.
- (8) Unwin, N. *J Mol Biol* **2005**, *346*, 967-89.
- (9) Unwin, N.; Miyazawa, A.; Li, J.; Fujiyoshi, Y. *J Mol Biol* **2002**, *319*, 1165-76.
- (10) Bouzat, C.; Gumilar, F.; Spitzmaul, G.; Wang, H. L.; Rayes, D.; Hansen, S. B.; Taylor, P.; Sine, S. M. *Nature* **2004**, *430*, 896-900.
- (11) Chakrapani, S.; Bailey, T. D.; Auerbach, A. *J Gen Physiol* **2004**, *123*, 341-56.
- (12) Kash, T. L.; Dizon, M. J.; Trudell, J. R.; Harrison, N. L. *J Biol Chem* **2004**, *279*, 4887-93.
- (13) Kash, T. L.; Jenkins, A.; Kelley, J. C.; Trudell, J. R.; Harrison, N. L. *Nature* **2003**, *421*, 272-5.
- (14) Kash, T. L.; Kim, T.; Trudell, J. R.; Harrison, N. L. *Neurosci Lett* **2004**, *371*, 230-4.
- (15) Kash, T. L.; Trudell, J. R.; Harrison, N. L. *Biochem Soc Trans* **2004**, *32*, 540-6.
- (16) Lee, W. Y.; Sine, S. M. *Nature* **2005**, *438*, 243-7.
- (17) Lummis, S. C.; Beene, D. L.; Lee, L. W.; Lester, H. A.; Broadhurst, R. W.; Dougherty, D. A. *Nature* **2005**, *438*, 248-52.
- (18) Xiu, X.; Hanek, A. P.; Wang, J.; Lester, H. A.; Dougherty, D. A. *J Biol Chem* **2005**, *280*, 41655-66.
- (19) Nowak, M. W.; Gallivan, J. P.; Silverman, S. K.; Labarca, C. G.; Dougherty, D. A.; Lester, H. A. *Methods Enzymol* **1998**, *293*, 504-29.
- (20) Cashin, A. L.; Petersson, E. J.; Lester, H. A.; Dougherty, D. A. *J Am Chem Soc* **2005**, *127*, 350-6.
- (21) Cashin, A. L.; Torrice, M. M.; McMenimen, K. A.; Lester, H. A.; Dougherty, D. A. *Biochemistry* **2007**, *46*, 630-9.
- (22) Zhong, W.; Gallivan, J. P.; Zhang, Y.; Li, L.; Lester, H. A.; Dougherty, D. A. *Proc Natl Acad Sci U S A* **1998**, *95*, 12088-93.
- (23) Jha, A.; Cadugan, D. J.; Purohit, P.; Auerbach, A. *J Gen Physiol* **2007**, *130*, 547-58.
- (24) Kearney, P. C.; Nowak, M. W.; Zhong, W.; Silverman, S. K.; Lester, H. A.; Dougherty, D. A. *Mol Pharmacol* **1996**, *50*, 1401-12.